Mechanism of actin polymerization revealed by cryo-EM structures of actin filaments with three different bound nucleotides

Steven Z. Chou[1] and Thomas D. Pollard[1,2,3,*]

[1]Department of Molecular Cellular and Developmental Biology
[2]Department of Molecular Biophysics and Biochemistry
[3]Department of Cell Biology
Yale University, PO Box 208103
New Haven, CT 06520-8103 USA

Supplemental materials

www.pnas.org/cgi/doi/10.1073/pnas.1807028116

Supplemental Table 1. Comparison of actin filament structures.

Sample (rabbit or chicken skeletal muscle actin except as noted)	Ligands	Confor-mation	Cryo-EM with direct detector except as noted	Resolu-tion (Å)	Year	Reference
Ca-ADP-actin in 2 mM $MgCl_2$		ADP	X-ray fiber diffraction	8.4	1990	Holmes (1)
Ca-ADP-actin	Gelsolin	ADP	X-ray fiber diffraction	3.3-5.6	2009	Oda (2)
Mg-ADP-actin		ADP	Energy filter, CCD camera	6.6	2010	Fujii (3)
Mg-ADP-actin	Coronin	ADP	CCD camera	8.6	2010	Ge (4)
Mg-ADP-BeF_x-actin	Coronin	ADP	CCD camera	8.6		Ge (4)
Ca-ADP-actin in 1 mM $MgCl_2$		ADP		4.7	2015	Galkin (5)
Ca-ADP-actin in 2 mM $MgCl_2$	Tropomyosin	ADP	Drift correction	3.7	2015	von der Ecken (6)
Ca-ADP-actin in 2 mM $MgCl_2$	Tropomyosin	ADP	Drift correction	3.6	2016	von der Ecken (7)
Ca-ADP-human γ–actin in 2 mM $MgCl_2$	Tropomyosin, myosin-II	ADP	Drift correction	3.7, 3.9	2016	von der Ecken (7)
Mg-ADP-actin	Phalloidin, ADP-myosin-I	ATP	Drift correction	3.3 - 3.9	2018	Mentes (8)
Mg-AMP-PNP-actin		ATP	Energy filter, phase plate, drift correction	3.4	2018	Chou (9)
Mg-ADP-P_i-actin		ATP	Energy filter, phase plate, drift correction	3.4	2018	Chou (9)
Ca-AMP-PNP-actin in 2 mM $MgCl_2$		ATP	Drift correction	3.6	2018	Merino (10)
Ca-ADP-BeF_x-actin in 2 mM $MgCl_2$		ATP*	Drift correction	3.4	2018	Merino (10)
Ca-ADP-P_i-actin in 2 mM $MgCl_2$		ATP	Drift correction	3.3	2018	Merino (10)
Ca-ADP-P_i-actin in 2 mM $MgCl_2$	Jasplakinolide	ATP*	Drift correction	3.7	2018	Merino (10)
Ca-ADP-actin in 2 mM $MgCl_2$		ADP	Drift correction	4.1	2018	Merino (10)
Ca-ADP-actin in 2 mM $MgCl_2$	Jasplakinolide	ATP*	Drift correction	3.6	2018	Merino (10)
Ca-ADP-actin in 2 mM $MgCl_2$	Cofilin	Cofilin	Drift correction	3.8	2018	Tanaka (11)
Mg-ADP-actin		ADP	Energy filter, drift correction	3.6		Present paper
Mg-AMP-PNP-actin		ATP	Energy filter, drift correction	3.1		Present paper
Mg-ADP-P_i-actin		ATP	Energy filter, drift correction	3.1		Present paper

ATP* indicates an obvious alternative path for the D-loop

Supplemental Table 2. Statistics for data acquisition and model refinement

	AMPPNP-actin	ADP-P_i-actin	ADP-actin
Image collection and processing			
Pixel size (Å)	1.045	1.045	1.045
Number of grids	1	1	1
Number of micrographs (final)	1308	1502	941
Number of particles (final)	310,826	411,164	123,806
Box size (pixels)	328	328	328
Particle distance (pixels; subunits)	26; 1	26; 1	26; 1
Map symmetry (rise, Å; twist, °)	27.40; -166.61	27.42; -166.56	27.45; -166.55
Resolution (overall, Å)	3.1	3.1	3.6
Accuracy of rotations (°)	0.92	0.92	1.04
Accuracy of translations (pixels)	0.40	0.40	0.40
Applied B-factor (sharpening)	-114.82	-99.71	-113.97
Model refinement			
Model to map correlation	0.80	0.81	0.81
RMS (bonds, Å)	0.01	0.01	0.01
RMS (angles, °)	1.00	1.00	0.94
Molprobity clash score	3.77	5.40	5.28
Ramachandran favored (%)	95.37	94.55	94.82
Ramachandran allowed (%)	4.63	5.45	5.18
Ramachandran outliers (%)	0.00	0.00	0.00
Rotamer outliers (%)	0.00	0.00	0.00

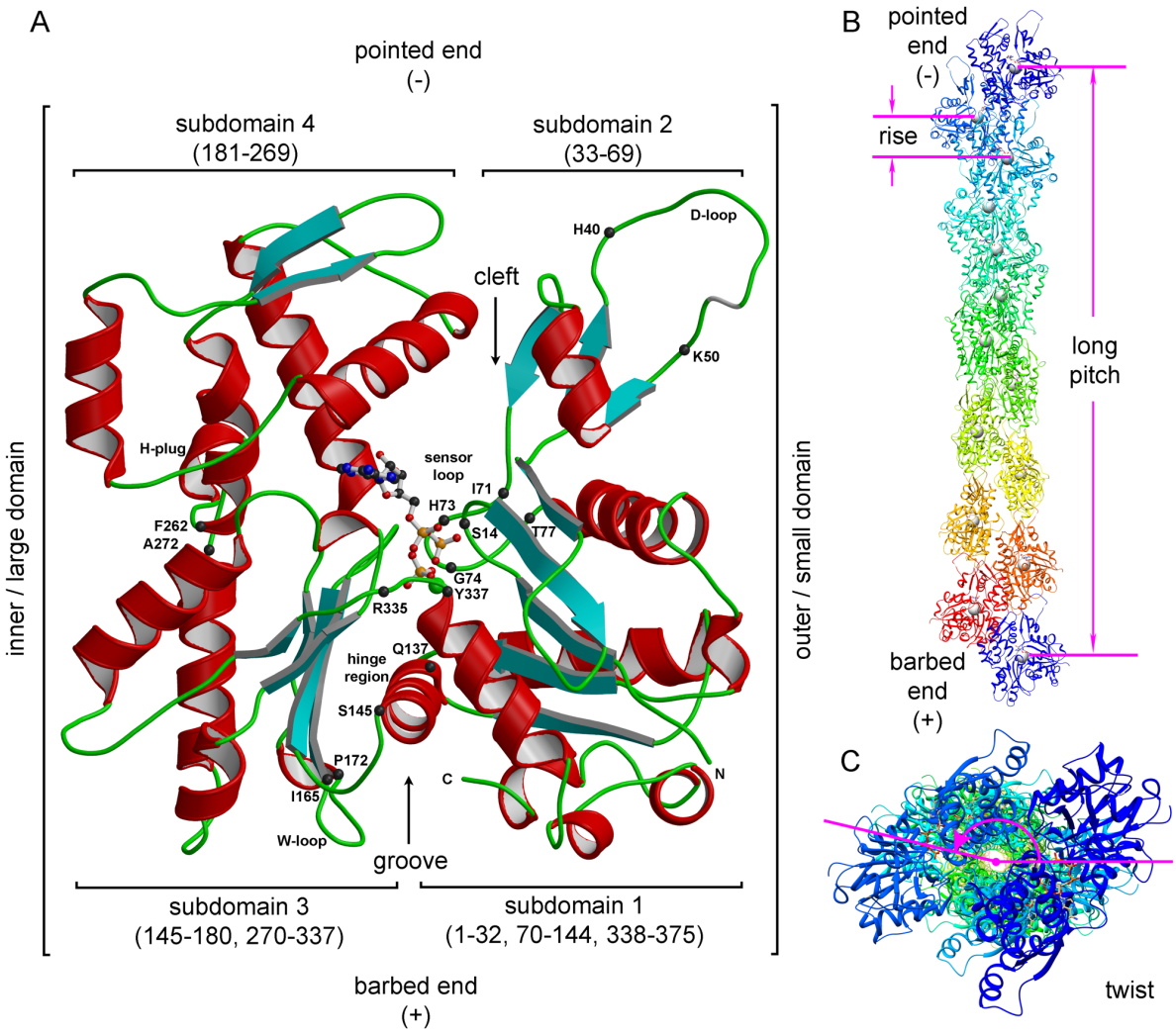

Figure S1. Structural elements of actin subunits and helical assembly of actin filaments. (A) Structural elements on an ADP-P_i-actin subunit. The DNase I-binding loop (D-loop; residues 40-50), sensor loop (residues 71-77), WH2-domain binding loop (W-loop/Y169-loop; residues 165-172), hydrophobic plug (H-plug; residues 262-272) and hinge region (hinge helix: residues 137-145; hinge loop: residues 335-337) are highlighted. (B) Helical assembly of ADP- P_i-actin filament with 14 subunits (side view). The grey ball in each subunit indicates the center of mass of the subunit, which is very close to β-phosphate of the ADP molecule. The rise per subunit along the short pitch helix is 27.51 Å and half a turn along the long-pitch helix is ~360 Å. The barbed end is facing downward. (C) Top view (from pointed end to barbed end) of ADP- P_i-actin filament. The twist for our ADP- P_i-actin filament is -166.68° (minus sign: left-handed helix).

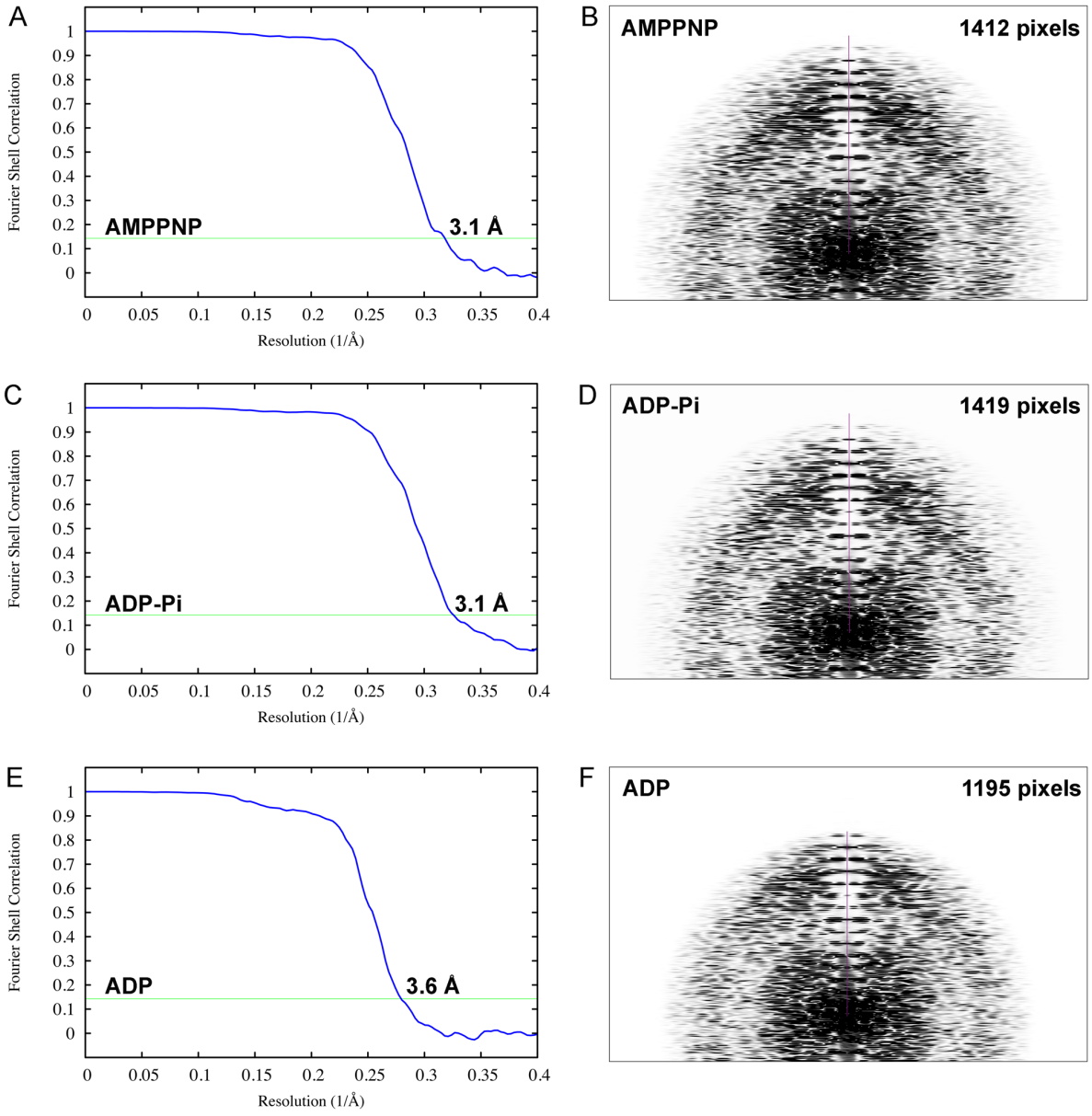

Figure S2. Global map resolution estimation. Resolution estimation of (A) AMPPNP-, (C) ADP-P_i-, and (E) ADP-actin reconstructions using Fourier Shell Correlation (FSC; blue curves) with 0.143 criterion (green horizontal lines). The resolutions are indicated in unit of angstroms. Resolution estimation of (B) AMPPNP-, (D) ADP-P_i-, and (F) ADP-actin reconstructions using layer-line images calculated from back projected images. The purple vertical line are the heights from the origin to the highest visible layer line in units of pixels. The layer-line images are 4096 × 4096 pixels, and the pixel size of back projected images is 1.045 Å. The resolutions are 3.03 Å for AMPPNP-actin filaments, 3.02 Å for ADP-P_i-actin filaments and 3.58 Å ADP-actin filaments using the formula: resolution = (pixel size) × (layer-line image size) / (layer-line height).

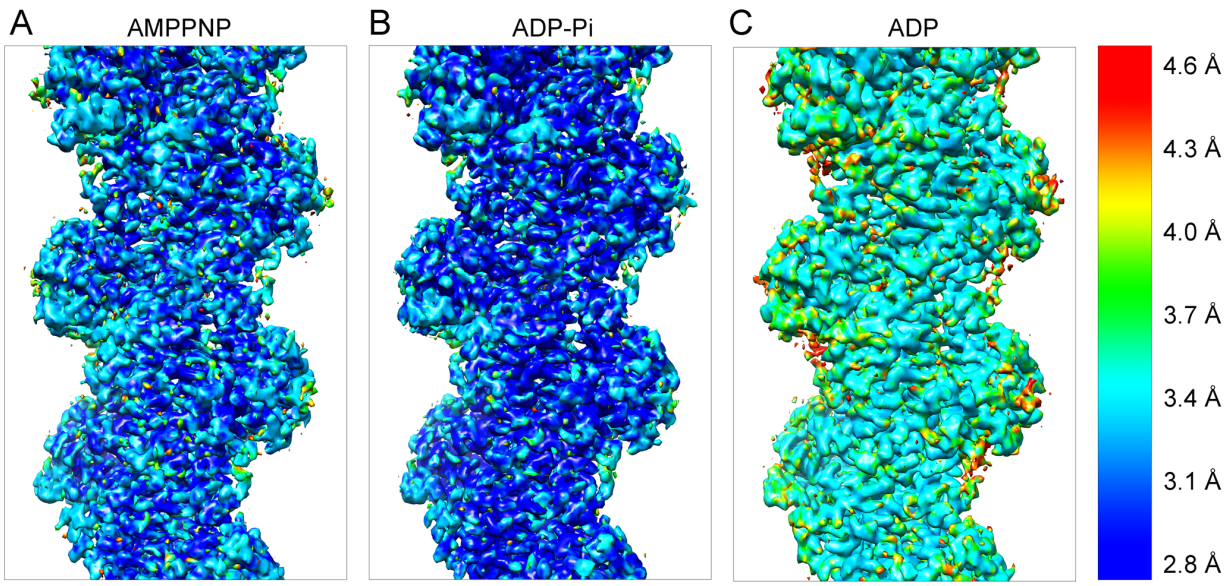

Figure S3. Local resolution estimated by ResMap (12) of the three actin filament reconstructions mapped onto the cryo-EM densities. (A) AMPPNP-actin, (B) ADP-P_i-actin, and (C) ADP- actin. The color-coded scale is on the right side.

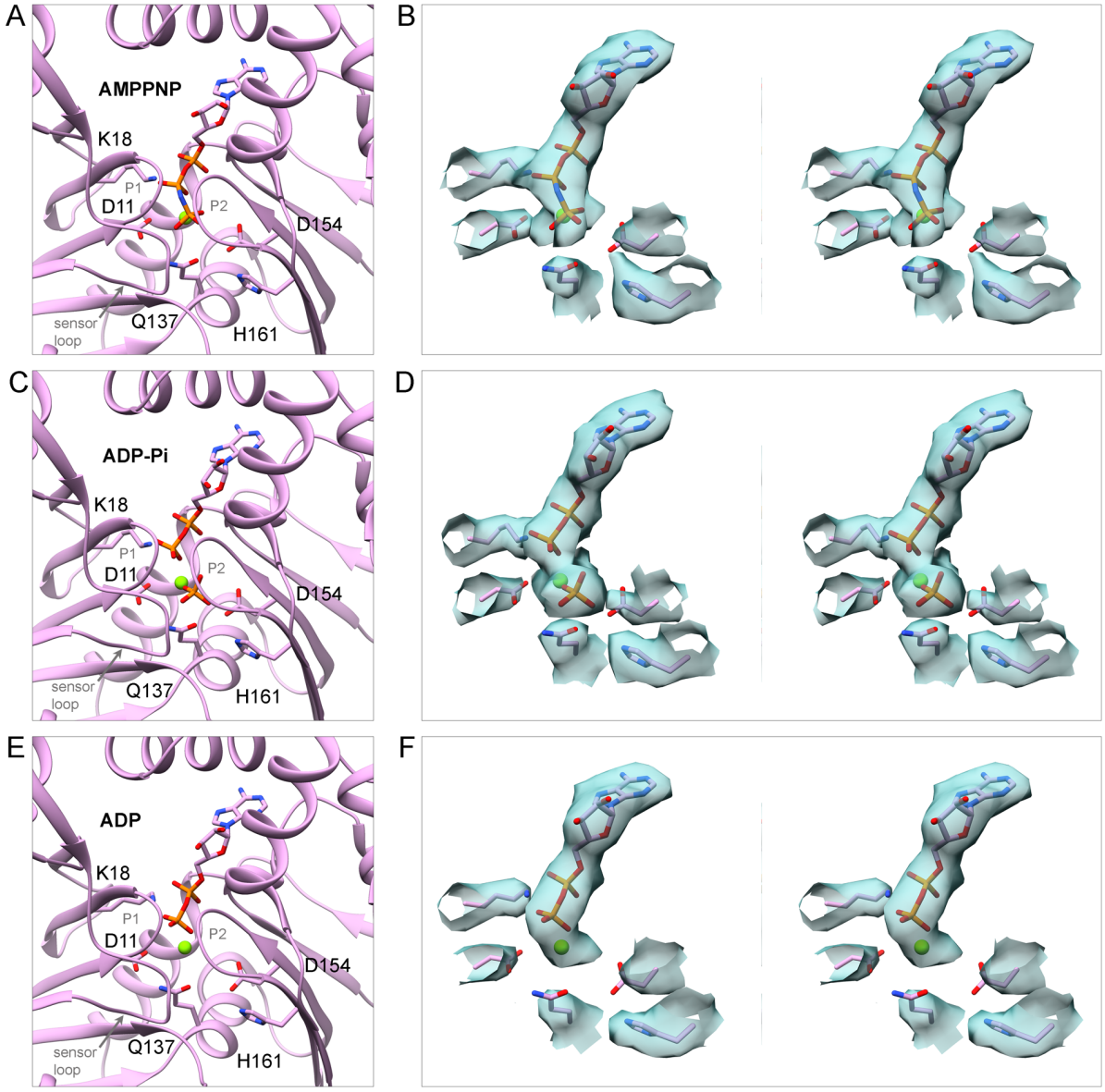

Figure S4. Structure of the active site during the ATPase cycle of polymerized actin. (A, B). AMPPNP-actin. (C, D) ADP-P_i-actin. (E, F) ADP-actin. Each row has two parts: (left) a ribbon diagram with stick figures and map densities zoned within 2.12 Å of the nucleotide and the important side chains D11, K18, Q137, D154 and H161; and (right) a wall-eye stereo view of the active site densities and stick figures of important side chains.

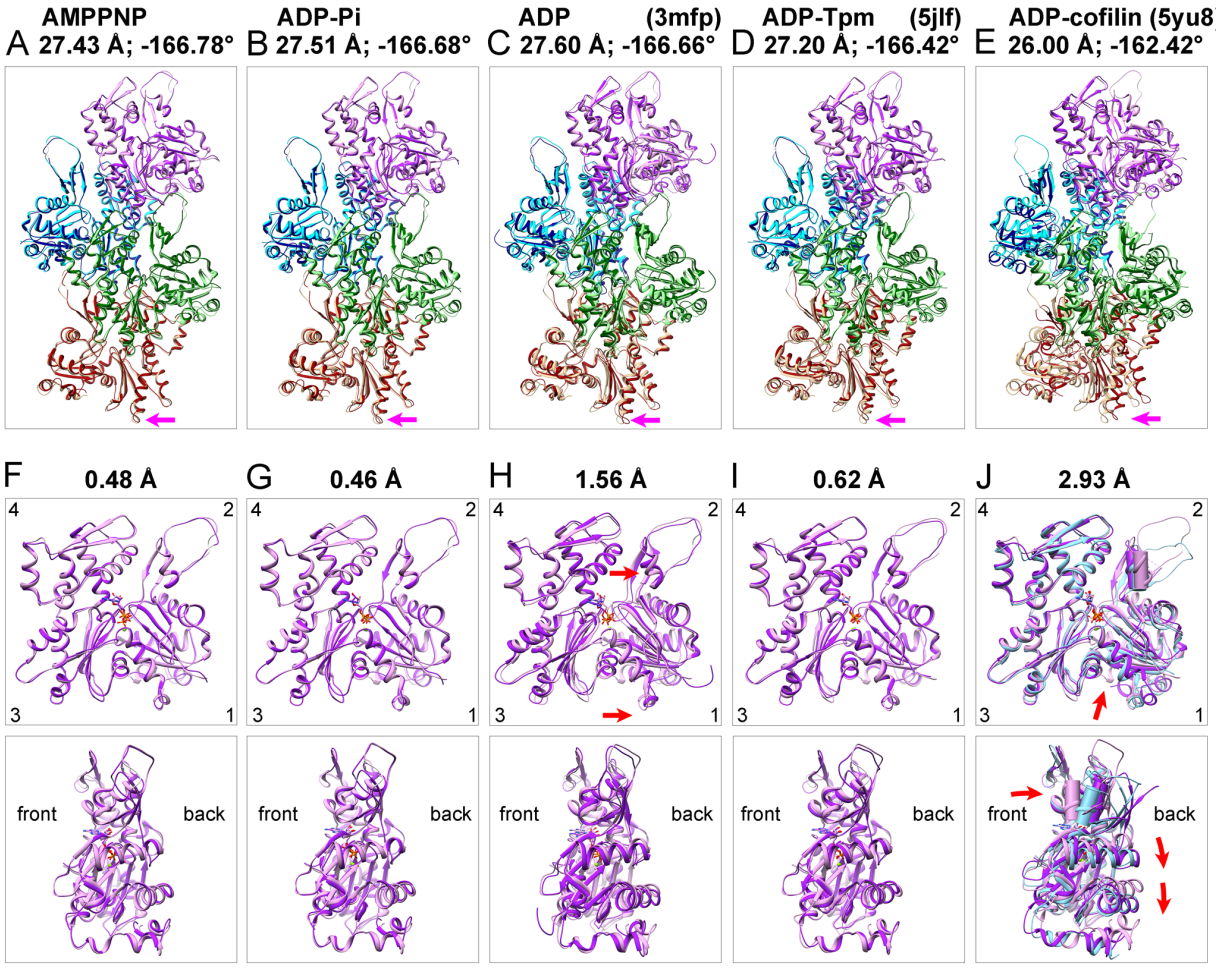

Figure S5. Ribbon diagrams comparing our ADP-actin filament model with five actin filament structures. The ADP-actin filament has a rise (subunit translation) of 27.53 Å and twist (subunit rotation) of -166.61° (minus sign: left-handed helix). (A-E) Superimpositions of four subunits from our ADP-actin filament model with the comparison filaments. The upper subunit of the ADP-actin filament was aligned with the upper subunit of each structure: (A) our AMPPNP-actin; (B) our ADP-P_i-actin; (C) ADP-actin (PDB: 3mfp); (D) tropomyosin-decorated ADP-actin (PDB: 5jlf); and (E) ADP-actin saturated with cofilin (PDB: 5yu8). The subunits in our ADP-actin structure are light colors (plum, cyan, light green and tan) and subunits in other structures are dark colors (purple, blue, dark green and dark red). The pink arrows point to a loop in subdomain 3 of the 4th (tan) subunit to show differences in subunit translation and rotation. (F-J) Superimpositions of the first subunit of our ADP-actin model with the first subunit in (A-E) after alignment of the Cα atoms in subdomains 3 and 4 (residues 145-337). The number at the top of each panel is the RMSD of Cα atoms of residues 5-370 relative to our ADP-actin structure, excluding the flexible regions (residues 1-4 and 45-49) in the N-terminus and D-loop. (J) Includes the crystal structure of an actin monomer (PDB: 2a42) in light blue. The only helix in subdomain 2 (residues 55-61) is rendered as a cylinder to compare inter-domain rotation angles. The red arrows point to structural differences (upper panel) and directions of motion (lower panel).

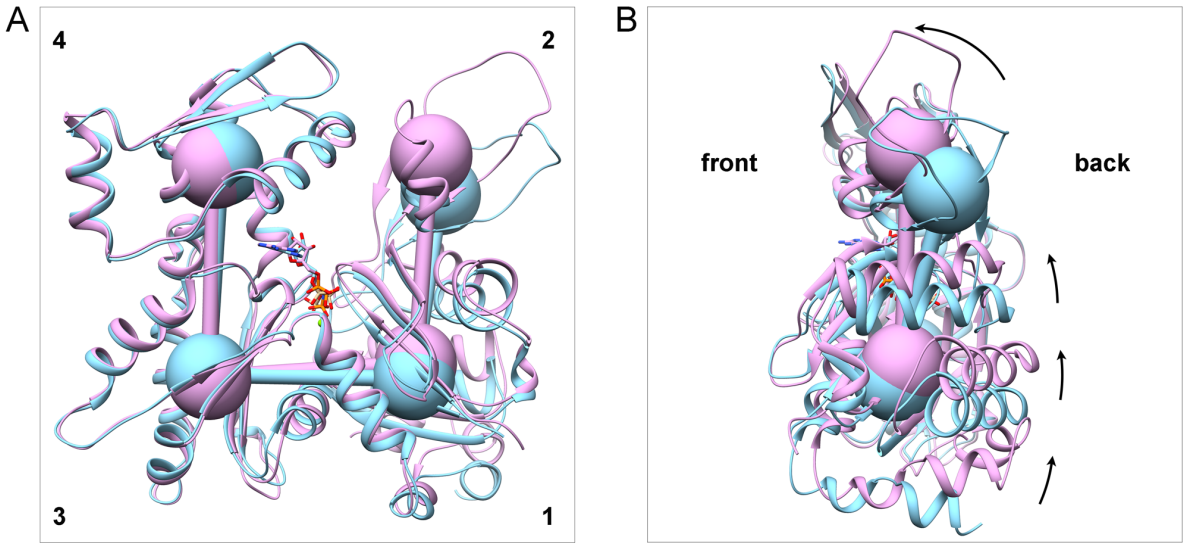

Figure S6. Inter-domain rotation and translation. (A) Front view and (B) side view of actin molecules. One actin subunit in our AMPPNP-actin filaments (plum) and one rabbit ATP-actin monomer (light blue) (PDB: 2a42) are superimposed after aligning subdomains 3 and 4. The balls indicate the centers of mass of subdomains. The primary sequences of these two molecules are the same.

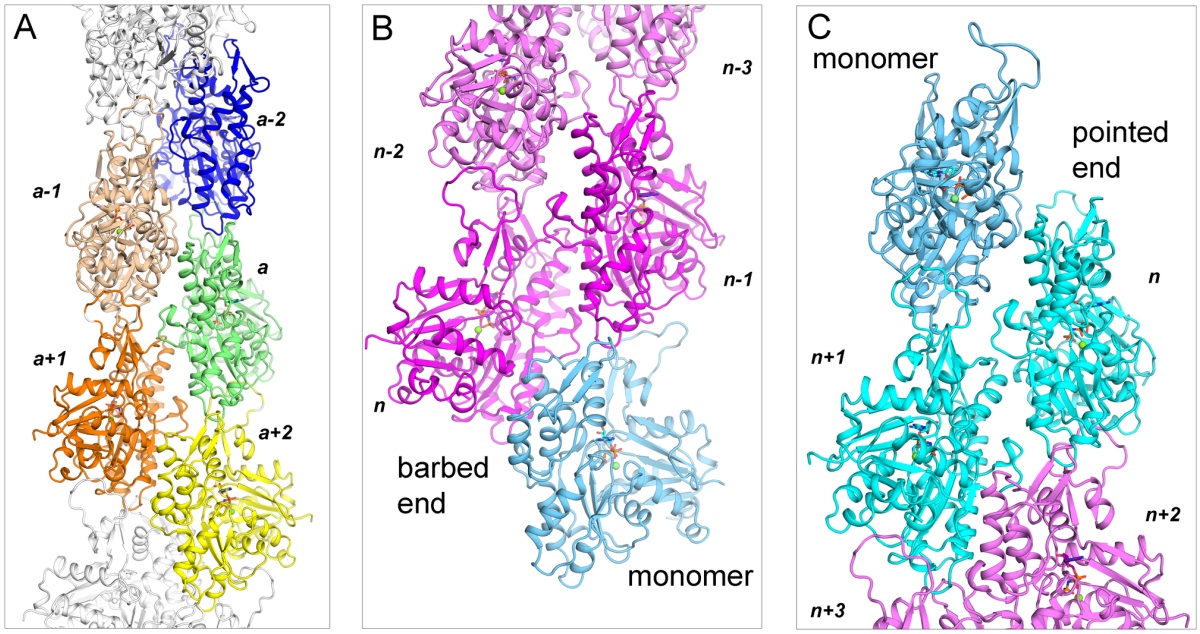

Fig. S7. Ribbon diagrams showing subunit interactions in filaments and possible conformations of subunits at the two ends. (A) Overview of filament showing contacts along the long-pitch helix (*a-2* to *a* to *a+2*) and interstrand contacts with two subunits along the short-pitch helix (*a-1* to *a* to *a+1*). (B) At the barbed end subunits *n* and *n-1* (magenta) likely have conformations similar to subunits in the middle of the filament (plum), because longitudinal contacts (between *n* and *n-2*, and between *n-1* and *n-3*) flatten these two subunits. The flattened conformation of these barbed end subunits is favorable for interactions with the pointed end of an incoming monomer (light blue). (C) At the pointed end, subunits *n* and *n+1* (cyan) are likely in a conformation similar to monomers with disordered D-loops, because longitudinal contacts (between *n* and *n+2* and between *n+1* and *n+3*) cannot flatten these two subunits. These conformations are unfavorable for interactions with an incoming action monomer, which is also in the unflattened conformation.

References

1. Holmes KC, Popp D, Gebhard W, & Kabsch W (1990) Atomic model of the actin filament. *Nature* 347(6288):44-49.
2. Oda T, Iwasa M, Aihara T, Maeda Y, & Narita A (2009) Nature of the globular to fibrous actin transition. *Nature* 457:441-445.
3. Fujii T, Iwane AH, Yanagida T, & Namba K (2010) Direct visualization of secondary structures of F-actin by electron cryomicroscopy. *Nature* 467:724–728.
4. Ge P, Durer ZA, Kudryashov D, Zhou ZH, & Reisler E (2014) Cryo-EM reveals different coronin binding modes for ADP- and ADP-BeFx actin filaments. *Nat. Struct. Mol. Biol.* 21:1075-1081.
5. Galkin VE, Orlova A, Vos MR, Schröder GF, & Egelman EH (2015) Near-atomic resolution for one state of F-actin. *Structure* 23:173-182.
6. von der Ecken J, *et al*. (2014) Structure of the F-actin-tropomyosin complex. *Nature* 519:114-117.
7. von der Ecken J, Heissler SM, Pathan-Chhatbar S, Manstein DJ, & Raunser S (2016) Cryo-EM structure of a human cytoplasmic actomyosin complex at near-atomic resolution. *Nature* 534:724-728.
8. Mentes A, *et al*. (2018) High-resolution cryo-EM structures of actin-bound myosin states reveal the mechanism of myosin force sensing. *Proc. Natl. Acad. Sci. U. S. A.* 115:1292-1297.
9. Chou SZ & Pollard TD (2018) Mechanism of actin polymerization revealed by cryo-EM structures of actin filaments with three different bound nucleotides. *bioRxiv* http://biorxiv.org/cgi/content/short/309534v1.
10. Merino F, *et al*. (2018) Structural transitions of F-actin upon ATP hydrolysis at near-atomic resolution revealed by cryo-EM. *Nat. Struct. Mol. Biol.* 25:528-537.
11. Tanaka K, *et al*. (2018) Structural basis for cofilin binding and actin filament disassembly. *Nat. Commun.* 10:1860.
12. Kucukelbir A, Sigworth FJ, & Tagare HD (2014) Quantifying the local resolution of cryo-EM density maps. *Nat Methods* 11(1):63-65.